LAMINAR AIRFOIL MODIFICATION ATTAINING OPTIMUM DRAG REDUCTION BY USE OF AIRFOIL MORPHING

Hiroharu Suzuki*, Kenichi Rinoie* and Asei Tezuka*
***Department of Aeronautics & Astronautics University of Tokyo, 113-8656, Japan**

Keywords: *Airfoil Morphing, Laminar Airfoil, Turbulent Transition, Drag Reduction*

Abstract

In this paper, the effectiveness of morphing a laminar airfoil's leading-edge through deformation in order to reduce the drag at the off-design angle of attack is herein investigated. The configuration of the airfoil was deformed under the structural restriction that the leading-edge is deformed while maintaining the girth of the deformed part and the configuration of the "wing box". The NACA 63_1-012 laminar airfoil was chosen as the original airfoil. The Reynolds number based on the original airfoil chord, was $Re_c = 3\times10^6$. Aerodynamic characteristics of the original and deformed airfoils have been investigated using a Viscous-Inviscid Interaction method. It is shown that the leading-edge deformation is effective in reducing the drag at the off-design angle of attack, in comparison to the original airfoil. The transition point has been estimated using a numerical method based on a linear stability theory. The deformation is an effective means to move the transition point aft on the airfoil, and the extension of the laminar flow area results in a reduction in the drag at the off-design angle of attack.

Nomenclature

C_d	drag coefficient
C_l	lift coefficient
C_p	pressure coefficient based on the free stream static and dynamic pressures
c	airfoil chord length, m
H	form factor
L	girth of the airfoil at the leading-edge, m
n	amplification factor
Re_c	Reynolds number based on the chord length
R_x	Reynolds number based on u_e and coordinate along the airfoil surface measured from the leading-edge
R_θ	Reynolds number based on u_e and θ
u_e	local velocity at the edge of the boundary layer, m/s
U_∞	free stream velocity, m/s
t	airfoil half-thickness distribution, m
x	Cartesian coordinate along the chord direction measured from the leading-edge of the original airfoil, m
y	Cartesian coordinate perpendicular to x and measured from the leading-edge, m
y_{camber}	airfoil camber line, m
Z	Cartesian coordinate parallel to x and non-dimensionalized using c as defined in eq. (2).
α	airfoil angle of attack, degree
δ	leading-edge deflection angle, degree
θ	momentum thickness, m

Subscripts

c	connecting point
L	center of rotation
0	leading-edge or original airfoil

1 Introduction

"Morphing aircraft" is one research topic that has been captivating the attention of the aeronautical science and engineering community. This involves aircraft that can

freely change shape during flight to attain the highest degree of performance and efficiency [1].

If the configuration of an airfoil is rigid, there is only one optimum flight condition (at the design angle of attack). Therefore, during other flight conditions, this airfoil's performance is compromised. However, by employing a morphing airfoil, the airfoil can conform to suit the optimum configurations required of different flight conditions such as at take-off, cruise and loitering, allowing for maximum performance and highly efficient flight. In previous studies, several researchers have been studying the morphing airfoil. Joshi and Tidwell[2] proposed a deforming wing platform. Prock *et al.*[3], and Gano and Renaud[4] proposed the deformation of an airfoil cross section. Martins and Catalano[5] discussed the variable camber airfoil employing the mission adaptive wing concept to optimize the transport aircraft wing under cruise conditions.

In this paper, we focus on a cross-sectional deformation of a laminar airfoil to reduce the drag at off-design angles of attack by use of this "morphing" technology.

Although a laminar flow airfoil gives a "laminar bucket" for the angle of attack range around a design point, laminar airfoils tend to have more drag than conventional airfoils at attack angles outside of the laminar bucket. With this background in mind, we propose that the drag of a laminar airfoil at its off-design angle of attack can be reduced if the boundary layer over its surface maintains its laminar properties as much as possible by deforming the airfoil with the help of airfoil morphing. The concept behind the laminar airfoil is that the transition is delayed when there is no adverse pressure gradient near the leading-edge and when the accelerating flow region is maintained as long as possible. However, at off-design angles of attack, this favorable accelerating region is lost and the transition is promoted. Our concept is to maintain this accelerative region of the original laminar airfoil even at off-design angles of attack, by deforming the leading-edge section suitably. A conceptual diagram for this drag reduction model is shown in Fig. 1. For a propeller driven aircraft, the lift coefficient C_l at which the rate of climb is maximized, is approximately 1.7 times greater than the C_l when the lift/drag ratio (L/D) is maximized. This means that significant drag reduction and increase in L/D are possible at an angle of attack larger than the design point when L/D is maximized.

However, from the structural point of view, the central part of an airfoil, which is the part between the front spar and the rear spar, is difficult to deform, because it constructs the torque box and comprises a fuel tank. Therefore, we have decided to deform only the leading-edge part anterior to the front spar. In addition, again from a structural point of view, we impose a constraint on the airfoil deformation so that the girth of the deformed airfoil's leading-edge part is kept equal to that of the original one. A conceptual diagram of this deformation is shown in Fig. 2.

Under these structural constraints, our research on aerodynamics has been carried out according to the flowchart shown in Fig. 3. First, the leading-edge part of the deformed airfoil is expressed analytically by the camber distribution and the thickness distribution, which are both functions of the chordwise stations. Next, the potential flow direct method is performed to estimate the surface pressure distribution on the deformed airfoil. Following this we select one particular deformed airfoil at each angle of attack whose surface pressure distribution satisfies the following three criteria: (1) It has no sharp suction pressure peak near the leading-edge; (2) The flow acceleration region is maximized along the chordwise direction; (3) It shows no discontinuity over the airfoil surface. Finally, the characteristics of this deformed airfoil are investigated by means of the Viscous Inviscid Interaction (VII) method which iterates the panel method and boundary layer analysis. The drag reduction resultant from enlargement of the laminar flow region is confirmed by an empirical transition point estimation and a numerical method based on a linear stability theory.

2 Analytical Method

2.1 Original Airfoil Shape

We selected the NACA63$_1$-012 laminar airfoil as the original airfoil to be used in this paper. This airfoil exhibits leading-edge stall characteristics at the Reynolds number of around 10^6. The shape of a laminar airfoil is described by coordinates of discrete data points listed in Ref.[6]. We obtained the geometry of the NACA63$_1$-012 laminar airfoil at a random arbitrary chord point by using cubic spline interpolations based on this data.

2.2 Airfoil Deformation

The following describes the methods employed for deformation of the airfoil's shape. A conceptual diagram of the deformation is shown in Fig. 4.

First we transfer the leading-edge point rotationally. The center of the rotational transfer is (x_r, y_r) and the rotational angle is δ. The leading-edge point (0, 0) is then transferred to (x_0, y_0). The deformed leading-edge and the original airfoil is connected at $x = x_c$. If the airfoil has a twin spar structure, the front spar is primarily located around x_c/c=0.25. In this research we fixed (x_r/c, y_r/c) as (0.25, 0), and the connecting point x_c/c as 0.25.

Next, we express the shape of the deformed leading-edge part using camber line y_{camber} and thickness distribution which is vertical to the camber line. The camber line y_{camber} and the half-thickness t are expressed in the following functions:

$$y_{camber}(Z)/c = A+BZ+CZ^2+DZ^3+EZ^4, \qquad t(Z)/c = FZ^{1/2}+GZ+HZ^2+IZ^3+JZ^4, \tag{1}$$

where

$$Z = (x-x_0) / c. \tag{2}$$

Then the values of ten coefficients, from A to J, are determined by the following restrictions as a function of only one parameter, rotation (deflection) angle δ.

1) $A=y_0/c$
2) The leading-edge radius is assumed to be the same as that of the original airfoil. (This condition determines the value F.)
3) Both the upper and lower surfaces of the airfoil must be continuous at the connecting point ($x = x_c$). This means the first-order and second-order derivative distributions are continuous at the connecting point. For this purpose we have to set some derivatives of the camber and thickness distributions (y_{camber}, y'_{camber}, y''_{camber}, y'''_{camber}, t, t' and t'') to be continuous at the connecting point. This condition specifies the values, from B to E, as shown in eq. (3). The values, from H to J, are specified as a function of G, as shown in eq. (4), where $Z_c = (x_c-x_0) / c$, $Y_c = y_{camber}(Z_c) / c$ and $T_c = t(Z_c) / c$.

$$\begin{pmatrix} Z_c & Z_c^2 & Z_c^3 & Z_c^4 \\ 1 & 2Z_c & 3Z_c^2 & 4Z_c^3 \\ 0 & 2 & 6Z_c & 12Z_c^2 \\ 0 & 0 & 6 & 24Z_c \end{pmatrix} \begin{pmatrix} B \\ C \\ D \\ E \end{pmatrix} = \begin{pmatrix} Y_c - A \\ \dfrac{dY_c}{dx} \\ \dfrac{d^2Y_c}{dx^2} \\ \dfrac{d^3Y_c}{dx^3} \end{pmatrix} \tag{3}$$

$$\begin{pmatrix} Z_c^2 & Z_c^3 & Z_c^4 \\ 2Z_c & 3Z_c^2 & 4Z_c^3 \\ 2 & 6Z_c & 12Z_c^2 \end{pmatrix} \begin{pmatrix} H \\ I \\ J \end{pmatrix} = \begin{pmatrix} T_c - \left(F\sqrt{Z_c} + GZ_c\right) \\ \dfrac{dT_c}{dx} - \left(\dfrac{F}{2\sqrt{Z_c}} - G\right) \\ \dfrac{d^2T_c}{dx^2} + \dfrac{F}{4Z_c^{\frac{3}{2}}} \end{pmatrix} \tag{4}$$

4) The structural condition that girth L of the deformed airfoil is the same as that of the original airfoil L_0, yields:

$$L=L_0. \tag{5}$$

To obtain the value of L numerically, we define it as the summation of the discrete panel lengths.

$$L \equiv \sum_{i=1}^{n-1} \sqrt{(x_{i+1} - x_i)^2 + (y_{i+1} - y_i)^2} \tag{6}$$

We obtained the deformed airfoil shape by finding the value G, which satisfies $L=L_0$ by use of Newton's method.

2.3 Potential Flow Direct Method

Smith and Hess's panel method [7] is used to obtain the surface pressure distribution in the preliminary discussion regarding the appropriateness of the present deformation. The number of the panel is 198, and the *x*-component of each panel length is determined as having half cosine distribution with smaller panels near the leading-edge. The angle of attack α is defined as the angle between uniform flow direction and the chord line of the original airfoil.

2.4 Viscous-Inviscid Interaction Method (VII)

After selecting the deformed airfoil configuration, we used the VII method based on Cebeci's Interactive Boundary Layer (IBL) method [8] to obtain the airfoil characteristics under viscous incompressible flow conditions. An overview of this method is as follows.

1) Smith and Hess's panel method with wake panels is used to obtain the external velocity distribution.
2) The viscous effects are incorporated into the panel method by distributing the blown air velocity across the airfoil surface.
3) Turbulent transition point was determined by the empirical correlation method. This method is based on Michel's method and Smith's e^9 method, and the correlation is described as the following equation:

$$R_\theta = 1.174\left(1+\frac{22400}{R_x}\right)R_x^{\,0.46}. \qquad (7)$$

4) The turbulence model used is Cebeci and Smith's zero equation model.
5) The drag coefficient is estimated by Squire and Young's method [9] as follows:

$$C_d = 2\left[\frac{\theta}{c}\left(\frac{u_e}{U_\infty}\right)^{\frac{H+5}{2}}\right]_{TE}, \qquad (8)$$

here, TE represents the trailing-edge.

6) Inverse boundary layer calculation is used over and posterior to the separated flow region.
7) The number of panels over the airfoil surface was 200 and that over the wake was 40. The *x*-direction length of the wake panel is 5 times longer than the original airfoil chord.
8) Convergence of the VII calculation was confirmed by the condition that the absolute value of the difference between the C_l value of present and previous steps is less than 0.0005.

2.5 Linear Stability Amplification Factor

Transition analysis is performed by use of the e^n method based on linear stability theory of the laminar boundary layer. The n-factor is defined as $\ln(A/A_0)$, where A_0 is the amplitude of disturbance at a neutral point and A is that for the amplification region in the downstream position. To estimate the onset of the transition chordwise position by the e^n method, it is necessary to give the n-factor when the transition occurs. This factor is referred to as N. However, since we do not know this empirical N value corresponding to the transition onset in our case, we estimate the chordwise n-factor distributions and try to discuss the differences between the n-factor distributions of the original wing and those of the deformed airfoil.

In this paper, the LSTAB code which was developed by Japan Aerospace Exploration Agency (JAXA), was used for this purpose. This code is based on the spatial linear stability theory of a three dimensional laminar boundary layer and can be used to estimate the amplification factor of disturbance and the n-factor chordwise distributions. Details of this LSTAB code are described in references [10] and [11].

3 Results and Discussion

3.1 Creation of Deformed Airfoil

As described before, the original airfoil used here is the NACA 63_1-012 airfoil. Its design angle of attack is 0°. The leading-edge of this airfoil was deflected using the methods described in Section 2.2. The maximum value of δ at which proper airfoil shape can be obtained, is present. This is because when δ is larger than this maximum value, G which

satisfies the structural conditions (see section 2.2 4)), ceases to exist. The maximum δ was 8.46° for the present deformation. The obtained leading-edge deformed airfoils for δ=0°, 2°, 4°, 6° and 8° are shown in Fig. 5.

3.2 Selection of Deformed Airfoil

The surface pressure distributions at α=2°, 4°, 6° and 8° obtained by the panel method are shown in Fig. 6. Each figure indicates that the pressure distribution changes as δ is increased. It can be explained that according to the increase in the deflection angle δ, the leading-edge pressure suction peak is reduced, and the minimum pressure point moves to the rearward position. However, when the angle of attack is larger than α=6° (Fig.6d, α=8°), the effectiveness of the present leading-edge deformation cannot be confirmed, i.e. the leading-edge pressure suction peak cannot be diminished at any rotation angle δ. Therefore, we decided to focus on angel of attack ranges of less than α = 6° in this study. In this angle of attack range, we selected the most desirable deformation angle δ for each α by changing δ every 0.2° from δ=0 to 8°. Here, the three criteria discussed in chapter 1 were applied when finding the δ value.

The selected pressure distributions are shown in Fig. 7a) and the pressure distributions of the original airfoil at the same α are shown in Fig. 7b). By comparing Figs. 7a) and 7b), it becomes evident that the present deformation would be an effective means in which to provide desirable pressure distribution, enlarging the laminar flow region at the off-design angle of attack of the original airfoil. This can be presumed so because the leading-edge's pressure suction peak is reduced and the flow acceleration area near the leading-edge is kept large. The distribution of selected δ versus α is shown in Fig. 8. This figure indicates that the larger the angle of attack α is, the larger the rotation angle δ needs to be. (Please be advised that the value of δ is selected from the "observed pressure distribution" and hence some scattering in this selection is inevitable). Figure 9 shows the selected deformed airfoil configurations for the angles of attack α = 2°, 4° and 6°.

3.3 VII Results

The characteristics of the original airfoil and the selected deformed airfoils were investigated by means of the VII method. The Reynolds number based on the original airfoil chord was $Re_c=3\times10^6$. The VII analysis was conducted at the selected δ for each α. The results are shown in Figs. 10-13. Figure 10 shows the drag polar of the original airfoil obtained by both experiment [7] and the VII method together with the drag polar of the present deformed airfoil obtained by the VII method. The VII results for the original airfoil in Fig.10a) show that there is a region where the C_d is relatively small at C_l = 0 – 0.3. This corresponds to the so called "laminar bucket". Regarding this bucket, there are slight differences between the experimental and VII results of the C_l when C_d jumps up at the right hand side of the bucket around 0.3. However, other features such as the minimum C_d and the C_d distribution outside of the bucket are quite similar between the VII and experimental results. Therefore, it can be said that the present VII method can validly estimate the C_l and C_d at different angles of attack. Figures 10b) and 10c) were obtained by the VII when the deflection angle δ was fixed and the angle of attack was altered (Fig.10b): δ=6°, Fig.10c): δ=6.6°). This means that optimized drag reduction has not been obtained for the entire range of C_l in these figures, but only at the design angle of attack. The vertical dotted lines in each figure indicate the design lift coefficient (i.e. design angle of attack) of each deformed airfoil. Figures 10 a)-c) show that as the design angle of attack increases, the lift coefficient region where the laminar bucket is observed moves toward the higher C_l value range, as is illustrated in Fig.1.

Figures 11-13 are the results of lift curve, polar curve and lift/drag ratio distributions for the present deformed airfoil when the optimum deflection angle was selected for each α.

Measured results of the original airfoil [7] are also plotted in Figs. 11 and 13.

When compared with the VII results and the experiments for the original airfoil in Fig.11, they indicate almost similar C_l at the same angle of attack. This means that the lift which decreases due to the deformation is very small, although the suction peak of the deformed airfoil is smaller than that of the original airfoil as Fig. 7 indicates.

As Fig. 12 shows, C_d of the "optimum" deformed airfoil is kept very low even at C_l values higher than C_l=0.3, at which C_d of the original airfoil increases suddenly. It is important to note that the deformed airfoil results in Fig.12 were plotted for the cases where the optimum deflection angle δ was selected for different angles of attack (i.e. different C_l). Thus, as shown in Fig.13 the lift/drag ratio increases drastically when $C_l > 0.3$. Fig.13 shows that the lift/drag ratio increases about 26% (from about 66 to about 83) at C_l = 0.5.

These results indicate that the present airfoil deformation is an effective way to reduce the drag coefficient and to increase the lift/drag ratio at the off-design lift coefficient for the original laminar airfoil.

The distribution of upper surface transition points that were estimated by the empirical correlation method in the VII are shown in Fig. 14. This figure indicates that the upper surface transition points of the deformed airfoil are kept rearward when compared with those of the original airfoil, by appropriately deflecting the leading-edge. It is thought to be the after-effect of this rearward-kept turbulent transition point, that the drag of the deformed airfoil is reduced compared to that of the original one.

3.4 Transition Analysis by e^n Method

In the previous section, although drag reduction was indicated, turbulent transition, which affects drag strongly, was estimated by empirical methods. Thus, to ensure that the present airfoil deformation model can effectively keep the transition point rearward, we estimated the value of linear stability amplification factor of the original and deformed airfoils by use of LSTAB code based on the e^n method. The results are shown in Fig. 15. This figure shows the chordwise distributions of the n-value for both the original and deformed airfoils at α=1°-6°.

Figure 15 indicates that the amplification factor (n-value) of the present deformed airfoil is kept smaller than that of the original airfoil at any chordwise station. The chordwise position where the amplification factor becomes positive and begins to increase moves in the upstream direction as the angle of attack is increased. Conversely, this same position for the deformed airfoil is almost fixed at the 10-15% chordwise position except where α=6°. These results suggest that the presently applied leading-edge deformation is an effective method to enlarge the laminar flow region.

As for Fig.15d) when α=4°, the n-value of the original wing could not be obtained downstream of the 1.4% chordwise position. This is because a laminar separation occurred at this position and the LSTAB code could not analyze the separated area. Due to the same reason, pertaining to the original wing, the n-values were only estimable near the leading-edge when α>4°. At α=6° (Fig.15f) the n-value of the deformed airfoil begins to increase very near to the leading-edge, just like the original wing. As can be seen in Fig.7a, there is a small area of negative pressure gradient at about 0.015c even for the deformed airfoil, which caused this rapid incremental increase of n.

It is often discussed that the transition n-value N can be selected as N = 9 regarding results reported from a wind-tunnel having normal free stream turbulent intensity. Although it is not clear whether this value is applicable for the present case, the transition point obtained by assuming N = 9 for the present analysis is plotted for each α in Fig.14b). For the original airfoil this figure shows that the transition point moves upstream abruptly as α is increased, but for the deformed airfoil the upstream movement of the transition point is moderate and this transition point is located downstream of the original airfoil even at high angles of attack,

except where α=6°. This tendency is quite similar to the results in Fig. 14a) in which Michel's method was applied. Therefore, it can be said that the transition point obtained by the VII is a reasonable one, and that the drag reduction obtained by the VII confirms the effectiveness of the leading-edge airfoil deformation reported in this study.

3.5 Structural Consideration

In this paper the leading-edge morphing was discussed from the perspective of aerodynamics. However, to accomplish such a morphing airfoil, structural study is also necessary. From the structural point of view, the possibility of such deformation as described in this paper has been examined [12]. By adding strain actuators both on the upper and lower surfaces of the leading-edge skin, the intention was to deform the airfoil by adding bending momemt induced by the actuators. Relationships between the location of the actuators and the deformation of the leading-edge were studied. In considering an airfoil with a 1m chord length and with skin thickness of 1mm at a Reynolds number of $3x10^6$, it was indicated that it is possible to deform the airfoil cross section similar to that in the present study, under the supposition that 20 actuators are located on the airfoil and if each actuator can produce 1.0% induced strain. However, it was reported that the maximum induced strain capacity of currently available actuators is limited to 0.2%. Further development of the actuators and structural analysis on the airfoil deformation are required.

4 Conclusions

To reduce the drag of a laminar airfoil at off-design angles of attack, the effect of leading-edge deformation by applying "morphing" technology was discussed in this paper. The NACA 63_1-012 airfoil was chosen as the original airfoil to be modified. The Reynolds number based on the original airfoil chord was 3×10^6. The deformation was done under the structural condition that only the leading-edge part is deformed while maintaining the "wing box" and that the girth of the deformed part is the same as that of the original one. An airfoil cross section with the expectation that its boundary layer will maintain its laminar properties at the off-design angle of attack, was selected based on the airfoil surface pressure distributions. By use of the Viscous-Inviscid Interaction method (VII), it was shown that such leading-edge deformation is an effective way to reduce drag when compared to values reported regarding the original airfoil at the off-design angle of attack. It was also confirmed by a numerical method based on linear stability theory that the deformation effectively keeps the transition point downstream compared with that of the original airfoil, to maintain the laminar flow region and therefore to reduce the drag at the off-design angle of attack. Thus, the drag reduction obtained by the VII confirmed the aerodynamic effectiveness of the present leading-edge airfoil deformation reported herein.

Acknowledgments

The authors gratefully acknowledge Dr. Kenji Yoshida and Mr. Yoshine Ueda of the Japan Aerospace Exploration Agency for their helpful support in conducting transition analysis and Prof. Takahira Aoki of the University of Tokyo for his advice on morphing airfoil structure.

References

[1] Wlezien R W, Horner G C, McGowan A R, Padula S L, Scott M A, Silcox R J and Simpson J O. The Aircraft Morphing Program. AIAA Paper 98-1927, 1998.

[2] Joshi S and Tidwell Z. Comparison of Morphing Wing Strategies Based Upon Aircraft Performance Impacts, AIAAPaper 2004-1722, 2004.

[3] Prock B C, Weisshaar T A and Crossley W A. Morphing Airfoil Shape Change Optimization with Minimum Actuator Energy as an Objective, AIAAPaper 2002-5401, 2002.

[4] Gano S E and Renaud J E. Optimized Unmanned Aerial Vehicle with Wing Morphing for Extended Range and Endurance, AIAAPaper 2002-5668, 2002.

[5] Martins A L and Catalano F M. Viscous Drag Optimization for a Transport Aircraft Mission Adaptive Wing, ICAS-98-2.3.2, Melbourne, Australia, 1998.

[6] Abbott I H and Von Doenhoff A E. *Theory of Wing Sections Including a Summary of Airfoil Data*. Dover Publications, New York, 1949.

[7] Moran J. *An Introduction to Theoretical and Computational Aerodynamics*. John Wiley & Sons, New York, 1984.

[8] Cebeci T. *Modeling and Computation of Boundary-Layer Flows*. Horizons Publishing, Long Beach, 1999.

[9] Squire H B and Young A D. The Calculation of the Profile Drag of Aerofoils, A.R.C. R&M No.1838, 1938.

[10] Yoshida K, Ogoshi H, Ishida Y and Noguchi M. Numerical Study on Transition Prediction Method and Experimental Study on Effect of Supersonic Laminar Flow Control. NAL SP-31, pp.59-79, 1996.

[11] Ueda Y, Ishikawa H and Yoshida K. Three Dimensional Boundary Layer Transition Analysis in Supersonic Flow Using a Navier-Stokes Code, ICAS2004-2.8.2, 2004.

[12] Tokuhiro M and Aoki T. On Structural Study of Wing Morphing, Proc. International Symposium on Innovative Aerial / Space Flyer Systems, P-16, Tokyo, Japan, Dec. 2004.

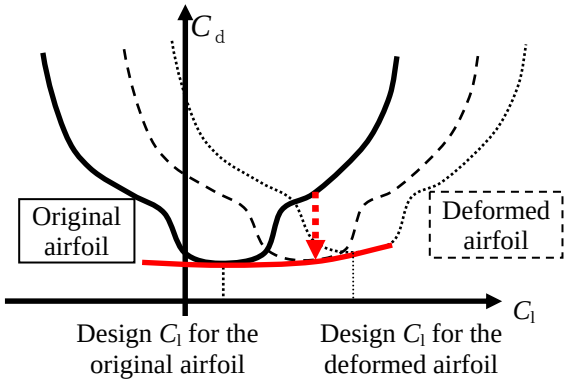

Fig. 1 Conceptual diagram of a drag reduction

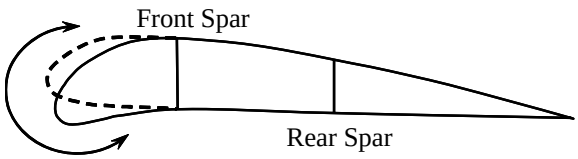

Girth: Constant

Fig. 2 Conceptual diagram of leading-edge deformation

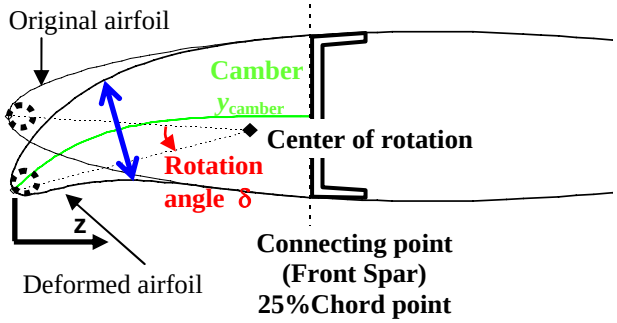

Fig. 4 Enlarged View of the Leading-edge deformation

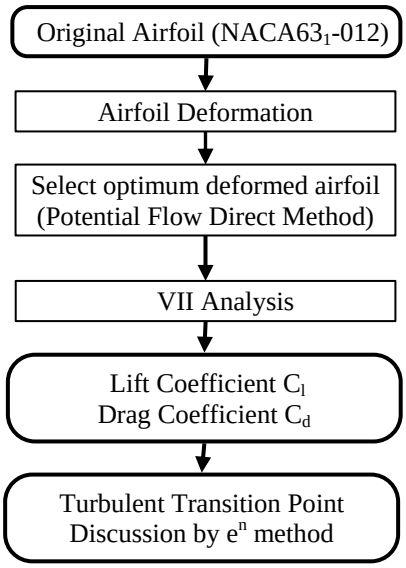

Fig. 3 Flowchart of the present research

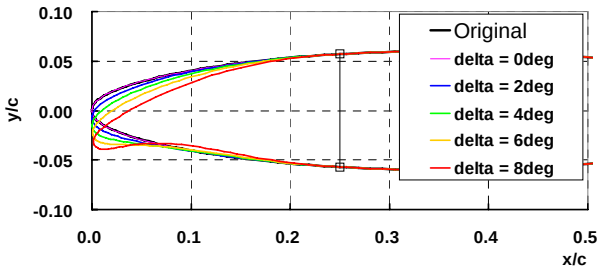

Fig. 5 Obtained deformed airfoils

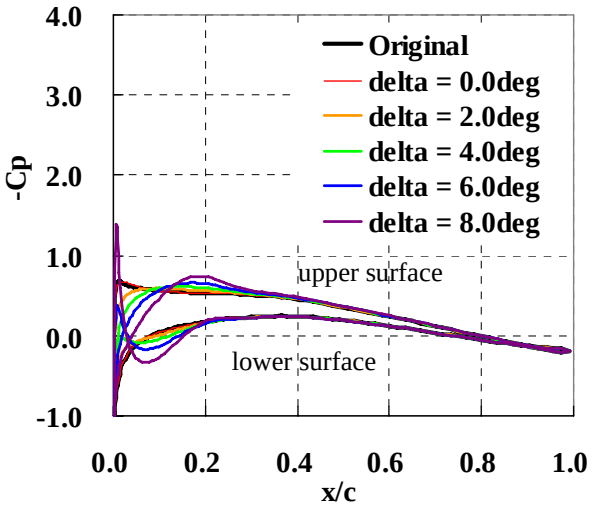

a) α=2°

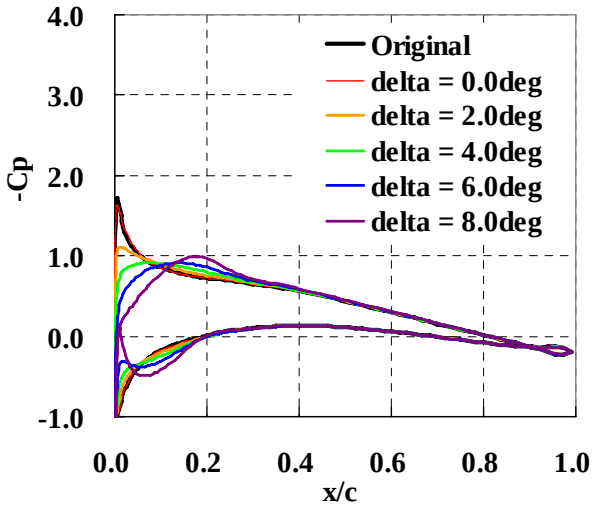

b) α=4°

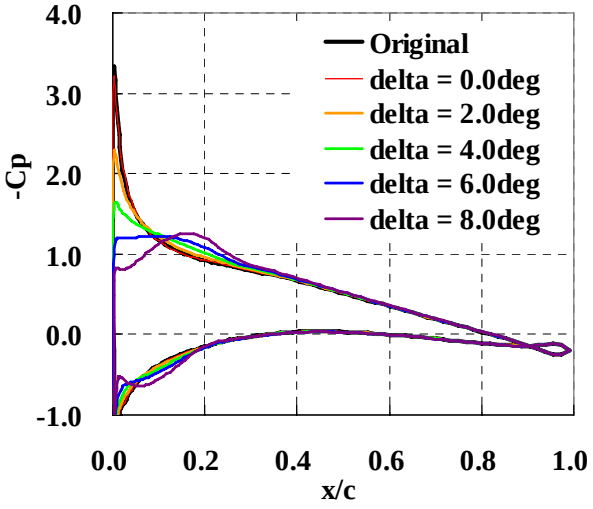

c) α=6°

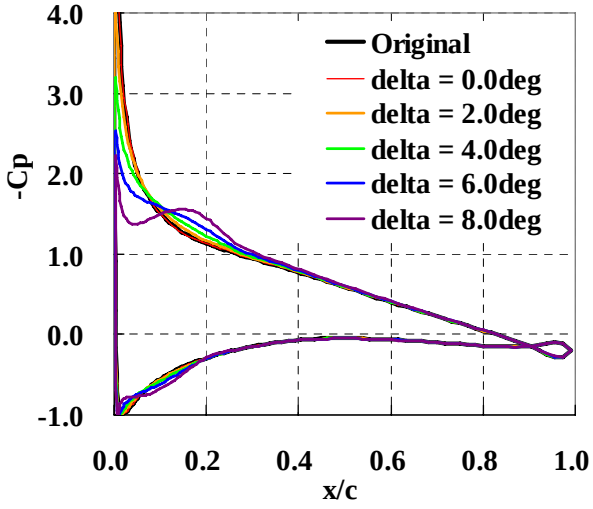

d) α=8°

Fig. 6 Pressure distribution shift caused by change of rotation angle δ

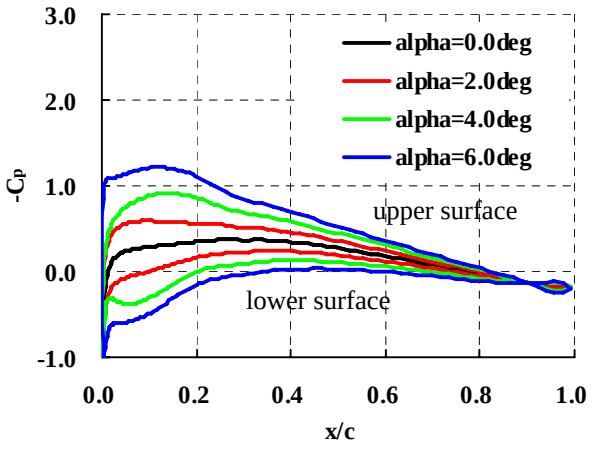

a) Selected pressure distributions of the deformed airfoil

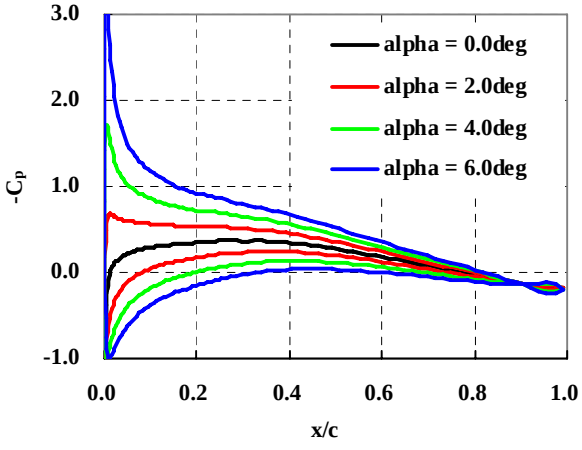

b) Pressure distributions of original airfoil

Fig. 7 Surface pressure distributions

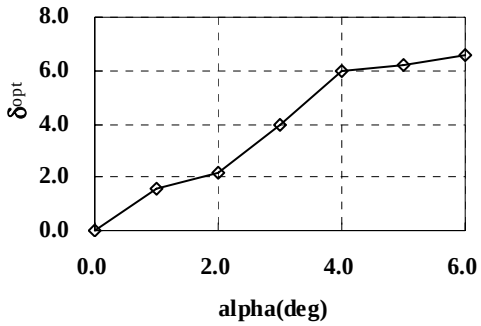

Fig. 8 Selected δ distribution versus α

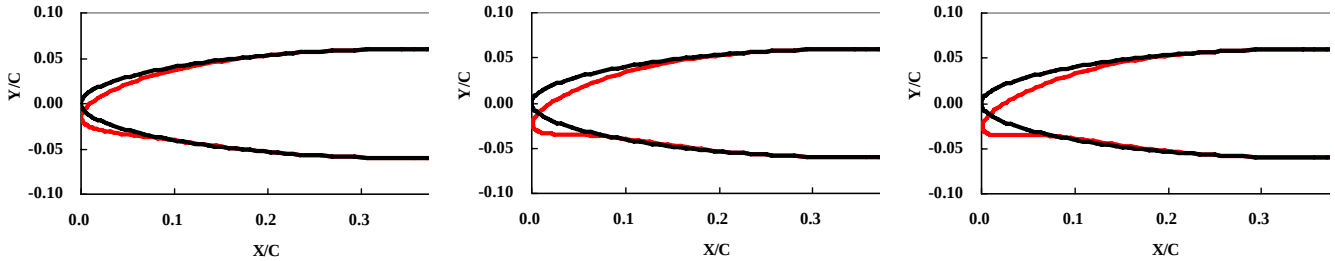

a) Selected for α=2° (δ=2.2°) b) Selected for α=4° (δ=6°) c) Selected for α=6° (δ=6.6°)

Fig. 9 Examples of selected deformed airfoils (Black line: Original airfoil, Red line: Deformed airfoil)

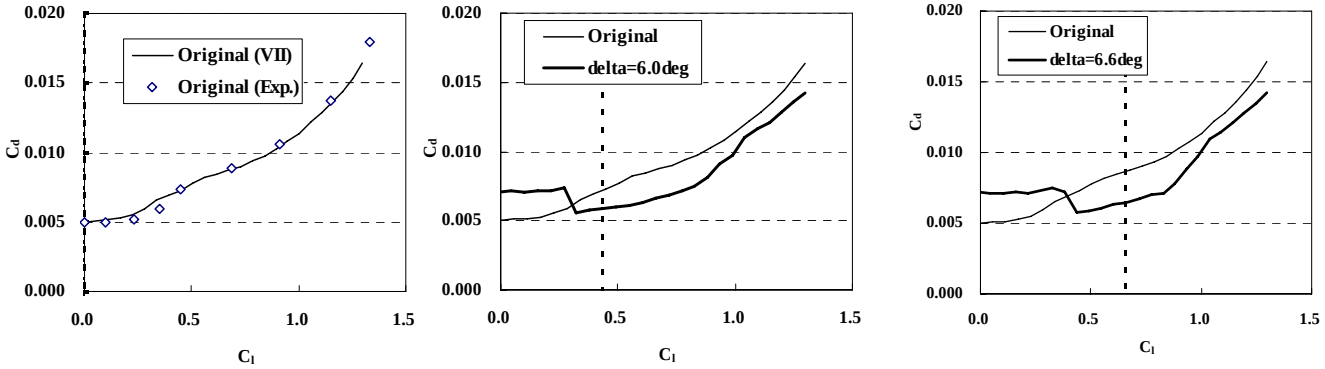

a) Original airfoil

b) δ=6° deformed airfoil (design angle of attack α=4°)

c) δ=6.6° deformed airfoil (design angle of attack α=6°)

Fig.10 VII Results – Drag Polar

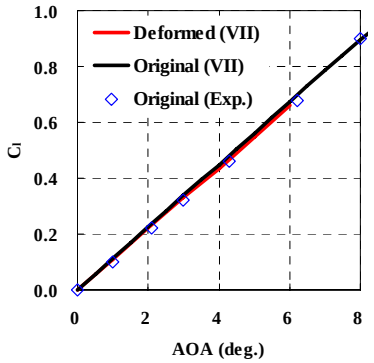

Fig. 11 C_l-α Curve

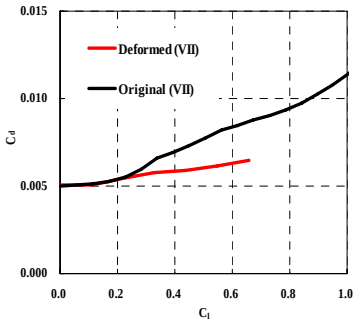

Fig. 12 Drag polar

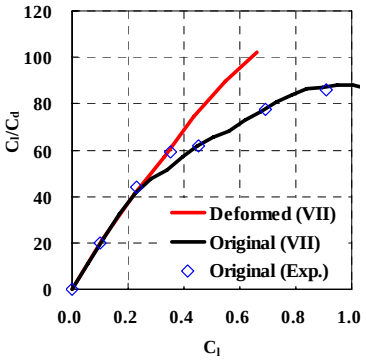

Fig. 13 lift/drag ratio distribution

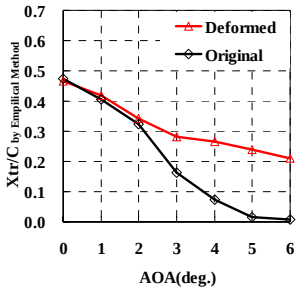

Fig.14a) Obtained by VII calculation (Empirical method)

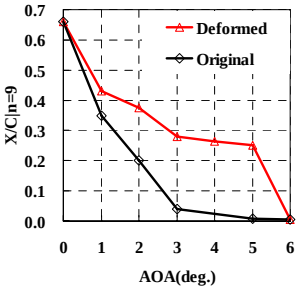

Fig.14b) Obtained by LSTAB code (e^n method)

Fig. 14 Upper surface transition points

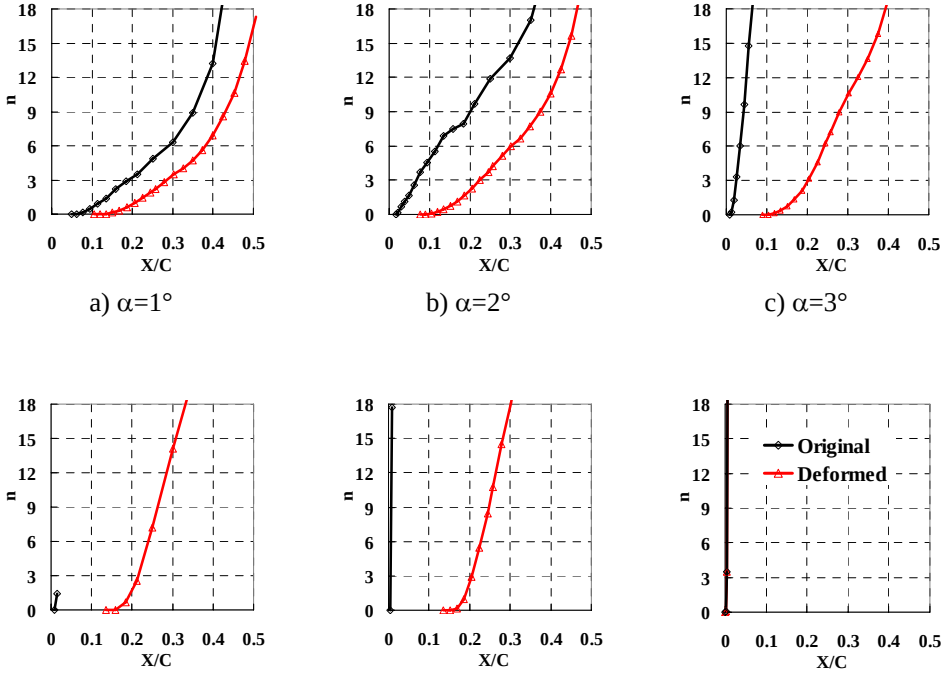

a) α=1° b) α=2° c) α=3°

d) α=4° e) α=5° f) α=6°

Fig. 15 Distributions of linear amplification factor n